Excitation Energies in Rare Isotopes as Indicators of Shell Evolution

Alexandra Gade
National Superconducting Cyclotron Laboratory and Department of Physics and Astronomy, Michigan State University, East Lansing, Michigan, USA

Introduction

The quest for a comprehensive and predictive model of atomic nuclei drives experimental and theoretical research endeavors around the world. The properties of short-lived, rare isotopes emerge as key ingredients for the development of nuclear models not only because they serve as crucial benchmarks for extrapolations into uncharted nuclear territory, but many important aspects of the interactions between the constituent nucleons are amplified in the regime of largely unbalanced proton and neutron numbers.

A quantitative understanding of the evolution of nuclear structure with respect to isospin is required to gain the ability to predict the properties of exotic nuclear systems that are not accessible for measurements in the laboratory, but that are crucial for an understanding of nucleosynthesis, for example. The nuclear potential and the resulting shell structure are fairly well established for stable nuclei. However, modifications of the structure of exotic nuclei have already been encountered: the emergence of new magic numbers and the breakdown of "canonical" shell gaps; intruder states of opposite parity descent from the next higher shell, crossing the shell gap and dominating the configurations of nuclei one shell down; and halo structures and skins occur at the threshold of nuclear binding in the proximity of the neutron drip line. Root causes are that for nuclei with extreme neutron-to-proton ratios, spin-isospin-dependent effects in the interaction are amplified [1, 2], and the proximity of the particle continuum in the regime of weak binding leads to exotic phenomena, for example, halo structures, skins, and cluster effects [3, 4].

Single-particle motion is one of the fundamental concepts to characterize the properties of nuclei. The single-particle levels of this fermionic quantum many-body system are grouped, forming the shell structure of the atomic nucleus [5, 6]. Large, stabilizing gaps occur between groups of single-particle states at certain, "magic" numbers of protons and neutrons (2, 8, 20, 28, 50, 82, 126). While the single-particle motion and the shell effects are determined by the nuclear mean field, collective phenomena result from configuration mixing by coherent parts of the residual interaction beyond the mean field.

A crucial experimental task is the quantitative assessment of modifications in the structure of nuclei from the measurement of observables that are calculable by theory and that signal structural change. Beyond the proof of existence of a rare isotope and the measurement of its ground-state half life, excited-state energies are often the first observables accessible in the laboratory. As will be outlined in the following, excitation energies indeed provide a sensitive probe of nuclear structure physics.

Simple Patterns in Complex Nuclei: Excitation Energies in Even-Even Nuclei—Often a First Glimpse

The energies of excited states offer a unique view into the structure of atomic nuclei. Excitation energies can be measured directly and in model independent ways and thus constitute prime observables that can be confronted with theory. For bound excited states, depending on their lifetime, prompt or delayed γ-ray spectroscopy is frequently used to extract excitation energies with great precision from measured transition energies. Excited states can be populated in nuclear reactions [7] or β decay [8], for example, exploiting the unique selectivity inherent to each of these different population mechanisms. The energies of very long-lived isomeric states can be accessed, for example, with Penning trap [9] or storage-ring [10] mass spectrometry. Energies of highly excited, particle-unbound states/resonances above the nucleon separation energy also provide interesting and important information, but are beyond the scope of this article (see Ref. [11], for example).

Nuclei with an even number of protons and neutrons—so-called even-even nuclei—have, without exception, a 0^+ ground state and most often a first excited state with total

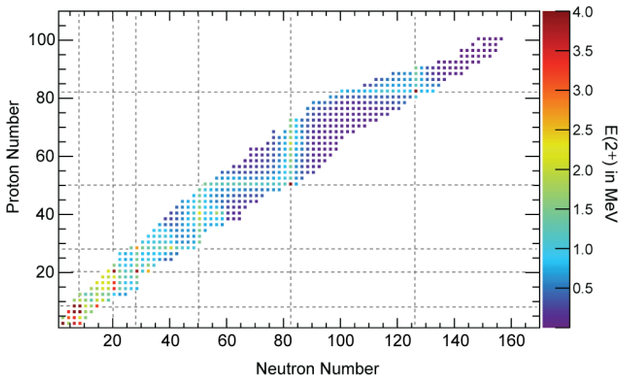

Figure 1. *The energy of the first 2^+ state as indicator of shell closures across the nuclear chart. Beyond N = 20 and Z = 20, increased 2^+ energies clearly indicate the canonical magic numbers, with the highest values attained for doubly magic combinations of protons and neutrons. In between shell closures, collectivity develops, signalled by low 2^+ energies. Figure adapted and updated from Refs. [12, 13].*

angular momentum and parity quantum number 2^+. The excitation energy, $E(2^+_1)$, sensitively reflects the structure of these nuclei and leads to strikingly clear patterns in the properties of this complex many-body system. Figure 1 shows the nuclear chart, even-even nuclei only, with the energy of the first 2^+ state color-coded.

In Figure 1, a pattern emerges beyond *N = 20* and *Z = 20* that with stunning clarity highlights the magic numbers of the nuclear shell model. Along the lines of the canonical shell gaps, the 2^+_1 energy is high, with the maximum values realized for doubly magic nuclei like ^{132}Sn and ^{208}Pb. Away from the shell closures, the 2^+_1 energies drop rapidly, indicating the onset of collective excitation mechanisms—rotations and vibrations, for example—where many valence protons and neutrons coherently participate in the excitations away from the stabilizing shell gaps. While this confirms the textbook shell-model predictions in a region where the most exotic isotopes have not yet been accessible, clear departures are visible for the lighter elements, where the spectroscopy of very neutron-rich isotopes has been enabled by present-generation rare-isotope facilities. Some of the most striking and prominent cases are discussed in the following.

The Rise and Fall of Magic Numbers

Figure 2 shows a cross-section of the nuclear chart of Figure 1. Displayed are the $E(2^+_1)$ energies of even-even Ca (*Z = 20*), Ar (*Z = 18*), S (*Z = 16*), Si (*Z = 14*) and Mg (*Z = 12*) isotopes from neutron number *N = 18* out to *N = 30* or the last known isotope of the respective chain [14]. The doubly magic character of ^{40,48}Ca is clearly visible from the high 2^+ energy. The local increase at *N = 20* for the Ar, S, and Si isotopic chains indicates that this shell gap is present also for these elements. In Mg, however, the 2^+ energy is substantially decreased beyond *N = 18*, signalling the breakdown of the neutron magic number *N = 20*. Similar behaviour is seen in the chain of Si isotopes at *N = 28*: ^{42}Si has the lowest-lying 2^+_1 state in this region.

The region around the neutron-rich nucleus ^{32}Mg has been one of the early and most important testing grounds of models or concepts that aim at describing shell evolution in neutron-rich nuclei (see [7, 15–16] and references within). Direct mass measurements of ^{31,32}Na revealed that the *N = 20* isotones in the vicinity of ^{32}Mg are more tightly bound than expected when assuming the presence of a *N = 20* neutron *sd*-shell gap. This effect could be reproduced in *deformed* Hartree–Fock calculations by filling of the neutron $f_{7/2}$ orbit. The identification of the low-lying 2^+_1 state of ^{32}Mg at 886(2) keV following the β-decay of ^{32}Na offered more evidence for an unexpected onset of collectivity. This observation as well could be explained by filling of the neutron $f_{7/2}$ intruder orbital for *Z < 14* in the framework of shell-model calculations. More generally, a deformed intruder configuration is formed by promoting two neutrons from the *sd* shell across the *N = 20* shell gap into the *fp* shell. For nuclei in this so-called "Island of Inversion" [15], the normal and intruder configurations are inverted with the strongly deformed intruder configuration $(sd)^{-2}(fp)^{+2}$

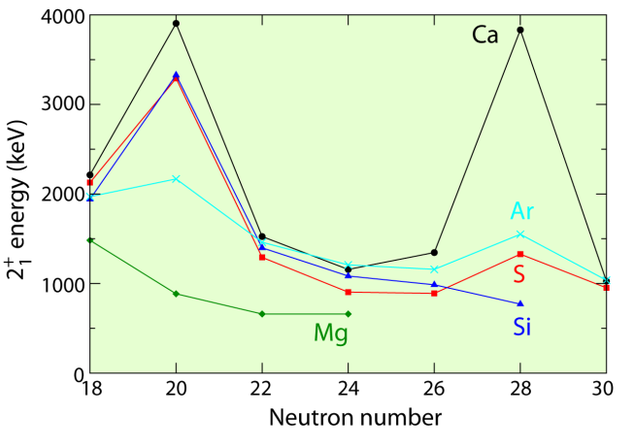

Figure 2. *The 2^+_1 energies in the Ca, Ar, S, Si, and Mg isotopic chains from N = 18 to N = 30. This systematics shows the disappearance of the N = 20 magic number in Mg and the breakdown of the N = 28 shell gap below Ca.*

descending to become the ground state. The mechanism behind this significant structural change that results in the disappearance of the $N = 20$ magic number has since been put into the larger context of shell evolution driven by the spin-isospin parts of the nuclear force, specifically the proton-neutron monopole parts of the tensor force, as recently reviewed by Otsuka and Schwenk [2]. A large body of experimental work has been mapping out the properties and extent of the "Island of Inversion" (see Refs. [7, 16] and references within), providing more benchmarks for theory in the quest to model shell evolution.

The key nucleus ^{42}Si has attracted much attention in recent years. The magic number 28 is of particular interest because it is the smallest of the canonical ones—and thus readily accessible by experiment and the most tractable by theory—whose existence mandates a strong spin-orbit interaction. Thus, in addition to the phenomenon of shell evolution, the breakdown of the $N = 28$ shell gap far from stability also provides information on the isospin dependence of the spin-orbit interaction. Experiments have shown that the $N = 28$ isotones ^{44}S ($Z = 16$) and ^{42}Si ($Z = 14$) are collective [17, 18], marking the breakdown of the $N = 28$ neutron shell closure below Ca. Also this disappearance of a magic number can qualitatively be explained by the monopole parts of the tensor force [1, 19] and enhanced quadrupole correlations across both the $Z = 14$ and $N = 28$ gaps [18, 20]. It is worth noting, however, that still today the consistent description of nuclei in the region around ^{42}Si remains a challenge for theory [19–23] with a lot more input required from experiment. The rich and detailed physics of this exotic mass region was recently featured in an article by Gaudefroy and Grévy [24].

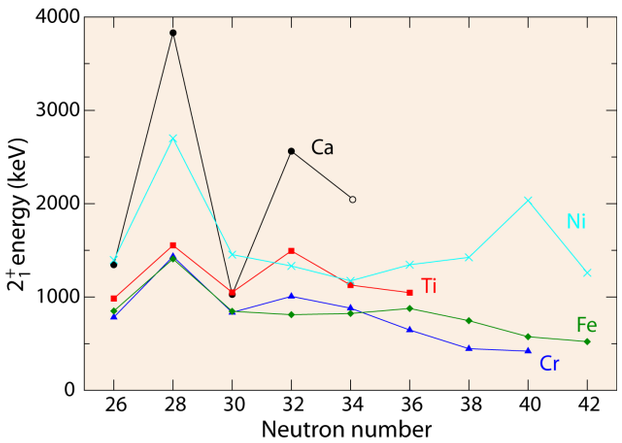

Figure 3. *Evolution of the 2^+_1 energies in Ca ($Z = 20$), Ti, Cr, Fe, and Ni ($Z = 28$) from neutron number $N = 26$ to $N = 42$. Taking the 2^+_1 energy as indicator of shell closures, this schematics shows the persistence of the $N = 28$ magic number, the emergence of a new shell gap at $N = 32$, and a significant change in the trends at $N = 40$, between Ni and Cr, which differ by just four protons (data from Refs. [14] and [29]).*

Consequences of shell evolution are not only the disappearance of canonical magic numbers but also the emergence of new shell gaps and the occurrence of rapid nuclear structure changes in localized regions of the nuclear chart. Figure 3 shows the 2^+_1 energies for the Ni, Fe, Cr, Ti, and Ca isotopic chains with neutron numbers ranging from 26 to 42 or the last known. The magicity of $N = 28$ seems undisputed from the systematics—a high 2^+_1 energy at doubly magic ^{48}Ca and slowly decreasing 2^+ energies as protons are added to magic $Z = 20$—while structural modifications become visible at neutron numbers $N = 32$ and $N = 40$.

The region of neutron-rich nuclei above doubly magic ^{48}Ca has provided much insight into the nature of the interactions responsible for changes in the shell structure. Evidence for an emerging sub-shell gap at neutron number $N = 32$ has accumulated over the past decade—notably from the elevated 2^+_1 excitation energies in ^{52}Ca [25], ^{54}Ti [26], and ^{56}Cr [27] shown in Figure 3. Large-scale shell model calculations, optimized for the description of *pf*-shell nuclei [28], attribute the onset of an $N = 32$ gap in neutron-rich Ca, Ti, and Cr nuclei to the combined actions of the neutron $p_{1/2}$–$p_{3/2}$ spin-orbit splitting and the weakening of the proton-neutron monopole interaction strength between $f_{7/2}$ protons and $f_{5/2}$ neutrons as Ca is approached. The experimental confirmation of the emerging $N = 32$ sub-shell gap resulting from the delicate interplay of the monopole part of the tensor force, which has been identified as a robust driver of shell evolution, and the magnitude of the $p_{1/2}$–$p_{3/2}$ spin-orbit splitting is a great success that showcases forefront experimental research and nuclear theory working in concert. The next benchmark in this region of the nuclear chart is the existence or non-existence of an $N = 34$ sub-shell gap in Ca which is predicted to be strong by some nuclear models. New results obtained at RIBF in RIKEN challenge this prediction with a comparably low-lying 2^+_1 state in ^{54}Ca [29]. The next key nucleus in the region is ^{60}Ca ($N = 40$), where an expected high neutron single-particle level density at the Fermi surface, originating from the descending $g_{9/2}$, $d_{5/2}$, $d_{3/2}$, and $s_{1/2}$ neutron orbitals [30], not only determines the nuclear structure but likely also the location of the neutron drip line in the Ca isotopic chain.

At slightly higher neutron number, the description of nuclei with $N = 40$ challenges theory as these isotones are

subject of particularly rapid structural evolution. Fueled by, among others, the deformation-driving neutron $g_{9/2}$ intruder orbital, they exhibit a remarkable variation in collectivity as a function of proton number: $N = Z = 40$ ^{80}Zr is strongly deformed [31], while at $Z = 28$, ^{68}Ni has a high-lying 2^+_1 state and reduced quadrupole collectivity [32] as one may expect for a magic number. With just two and four protons less than ^{68}Ni, the low first 2^+ excitation energies of ^{66}Fe and ^{64}Cr indicate yet another sudden change in the nuclear structure with increased collectivity, possibly the highest in the region [33, 34]. The neutron number $N = 40$ is of interest as it was conjectured early that ^{68}Ni ($Z = 28$, $N = 40$) may be doubly magic [35], with the $N = 40$ gap being a relic of the harmonic oscillator potential. In more realistic potentials, $N = 40$ is washed out by the effect of the strong spin-orbit interaction, favoring the occurrence of the $N = 50$ "spin-orbit" shell gap over the $N = 40$ oscillator magic number. At first glance, the high 2^+_1 excitation energy observed for ^{68}Ni may confirm the suspected double magicity; however, the systematics of two-neutron separation energies, S_{2n}, does not show any evidence for an increased $N = 40$ shell gap in this region [36]. The situation of ^{68}Ni is obviously more complicated and serves as a warning that, in a few cases, excitation energies are just one indicator and many more observables need to fall into place to firmly claim a sub-shell gap or a magic number. In ^{68}Ni, the high-lying 2^+_1 state together with the small electromagnetic transition strength for its excitation from the ground state is attributed to the fact that due to the change in parity between the *fp* shell and the $g_{9/2}$ orbital only neutron pairs can cross the $N = 40$ gap to form a 2^+ state, while the lower energy, one-neutron-one-hole configurations only can generate excited states of negative parity [32, 37]. The modeling of the rapid change in nuclear structure, from the strong deformation at $N = 40 = Z$ to the peculiar situation in ^{68}Ni and the sudden onset of collectivity in ^{66}Fe and ^{64}Cr, presents a formidable benchmark for nuclear structure calculations, where many effects that drive shell evolution and the emergence of collectivity need to be included properly.

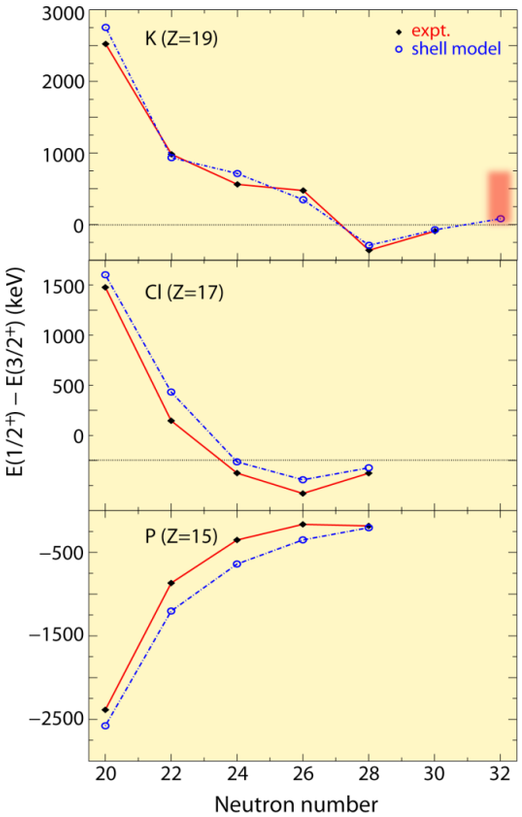

Figure 4. *Comparison of the measured $E(1/2^+_1)$-$E(3/2^+_1)$ energy splitting to shell model calculations for K, Cl, and P isotopes approaching neutron number 28. The ordering of the levels in ^{41}P and ^{45}Cl has not been determined unambiguously by experiment and is assigned by comparison with calculations. Tracking the energy splitting in this region not only provided a sensitive benchmark for shell model—with an excellent match of measurements and theory (SDPF-NR)—but also demonstrates the effect of correlations as explained in the text. Figure adapted from Ref. [39]; another well-matching comparison with a modified shell model interaction, SDPF-U, can be found in Ref. [20]. The values for N = 30, 32 in potassium are taken from Ref. [40]. While the sign of $E(1/2^+_1)$-$E(3/2^+_1)$ in ^{51}K was determined by the work reported in Ref. [39], the magnitude is still unknown as the excited $1/2^+$ state has not yet been found.*

Odd-Mass Nuclei

One nucleon away from a doubly magic nucleus, the low-lying level scheme typically resembles the single-particle spectrum, where the total angular momenta J of the ground state and the low-lying excited states are given by the total angular momentum of the single-particle orbits which the odd nucleon can occupy. Away from doubly magic shell closures, the low-lying structures of multi-valence nucleon systems are determined by a variety of nucleon-nucleon correlations. States of predominant single-particle or single-hole character can selectively be populated with nucleon-adding or removing transfer (or knockout) reactions—these states provide crucial information to understand the backbone of the nuclear shell model [38].

Figure 4 shows the evolution of the $E(1/2^+_1)$-$E(3/2^+_1)$ energy splitting in neutron-rich odd-Z K, Cl and P isotopes

with even neutron numbers from $N = 20$ to $N = 28$ [39]. In the limit of an extreme single-particle picture, the splittings at $N = 20$ and $N = 28$ in the potassium chain should correspond to the energy difference of the $s_{1/2}$ and $d_{3/2}$ single-proton orbitals. Proton-neutron correlations are reflected in the evolution of this energy splitting, however; in fact, uncovering a way to study these. The energy splitting in the potassium isotopes decreases significantly with two neutrons added to $N = 20$ due to the coupling of neutron excitations with the proton single-hole states—the pure single-particle character is lost [20]. The single-particle nature is recovered at $N = 28$, however, with the levels almost degenerate and the ordering reversed, indicating that the proton-neutron interaction is more strongly attractive between the proton $d_{3/2}$ and the neutron $f_{7/2}$ orbitals than between the proton $s_{1/2}$ and neutron $f_{7/2}$ orbitals [20]. Beyond $N = 28$, the neutron $p_{3/2}$ orbit is being filled and the stronger attraction between the neutron $p_{3/2}$ and proton $s_{1/2}$ orbitals leads to a "re-inversion" of the two states in ^{51}K [20]. This provides important insight into the shell evolution in the vicinity of $N = 28$ and poses a stringent benchmark for theory. For Cl and P the situation is more complicated as there are three and five proton holes relative to magic $Z = 20$, respectively. Inherent to all three chains is the near degeneracy of the $1/2^+$ and $3/2^+$ states at $N = 28$. This near degeneracy fuels SU(3) quadrupole correlations that are partly responsible for the onset of collectivity at ^{42}Si [18, 20]. The agreement between measured and shell-model energy splitting is excellent [20, 39], however, ^{51}K turns out to be a discriminating case with differing shell-model predictions for the magnitude of the energy splitting [40].

Odd-Odd Nuclei—The Most Demanding Challenge

Nuclei with an odd number of protons and neutrons—odd-odd nuclei—are particularly challenging for experiment as well as for theory. Due to the many different ways the odd valence protons and neutrons can couple, the level schemes of odd-odd nuclei are typically characterized by a high level density. Away from closed shells, the sequences of states cannot easily be constructed from angular-momentum coupling and simple arguments. The fine details of the proton-neutron interaction and the couplings within the proton and neutron valence spaces determine the excitation spectra. It is obvious that this poses a grand challenge to theory as many aspects of the nucleon-nucleon interaction and all underlying single-particle energies have to be treated properly to reproduce the properties of odd-odd systems. Figure 5 shows the example of ^{44}Cl ($Z = 17$, $N = 27$) and ^{46}Cl ($Z = 17$, $N = 29$) [41].

Figure 5 (left) displays the γ-ray spectra detected in coincidence with ^{44}Cl and ^{46}Cl produced in the fragmentation of a ^{48}K beam [41]. Many transition are visible that point to complex level schemes and a high level density. In contrast, Figure 6, which will be discussed in more de-

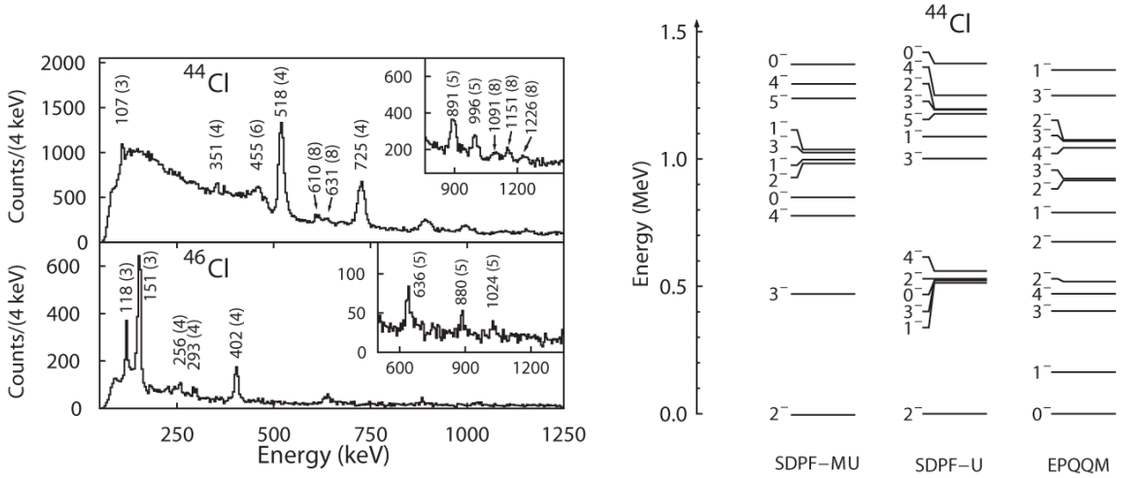

Figure 5. *Left: Gamma-ray spectra of the odd-odd neutron-rich nuclei ^{44}Cl and ^{46}Cl. Excited states in these nuclei were populated in the fragmentation of ^{48}K [42]. The large number of observed γ-ray transitions is indicative of the high level density typically observed in nuclei with an odd number of protons and neutrons. Right: ^{44}Cl shell-model calculations with three different effective interactions compared with each other. The complex γ-ray spectra and widely different shell-model predictions demonstrate the challenge that odd-odd nuclei pose for experiment as well as for theory. Figure adapted from Ref. [42] with SDPF-MU shell-model calculations [29] added.*

tail in the next section, shows the γ-ray spectrum of the even-even nucleus ^{36}Mg as populated in the two-proton removal from a ^{38}Si beam. The formidable challenge for theory is reflected by the fact that three different shell-model effective interactions, that employ the same model spaces, predict widely differing level schemes for ^{44}Cl. It is clear that J^{π} assignments are required from experiment, which is a challenge in the regime of low statistics inherent to the spectroscopy of rare isotopes and high level density.

Experimental Measurements—
The Example of In-Beam γ-Ray Spectroscopy

The excited states of the majority of the most neutron-rich nuclei in Figures 2 and 3 have been measured first with the method of in-beam γ-ray spectroscopy at rare-isotope facilities that use projectile fragmentation as a production mechanism of exotic nuclei. Examples are ^{42}Si [18] first measured at GANIL, the pioneering in-beam spectroscopy of ^{46}S [21], ^{36}Mg [42] and ^{64}Cr [34] performed at NSCL/MSU, and the excited states of ^{54}Ca [29] and ^{58}Ti [43] first reached at RIKEN.

These light and medium-mass nuclei far away from stability can be efficiently produced by fragmentation of stable beams impinging on stable targets at high energy. The resulting rare-isotope beams are then available for experiments at velocities typically exceeding 30% of the speed of light. Well-developed experimental techniques used for decades in the study of stable nuclei are rarely applicable in the regime of the low beam rates encountered for the shortest-lived nuclear species. Sensitive new experimental techniques have been developed to enable *in-beam* spectroscopic studies with fast rare-isotope beams [7]. Compared to stable beam rates, rare-isotope beams are typically less intense by several orders of magnitude. In-beam γ-ray spectroscopy compensates for the reduced beam rate by employing thick reaction targets. With that, advantage is taken of the high beam velocity (v/c > 0.3), realizing experiments with luminosities comparable to stable-beam experiments, however, at beam rates of up to a factor of 10^4 less. Nuclear reactions, for example Coulomb excitation or one- and two-nucleon removal reactions [7, 38], are induced in the collision with targets of thicknesses of the order of several hundred mg/cm^2. The detection of de-excitation γ-rays to identify the residue's final state or to tag the inelastic process in scattering events then reveals excitation level schemes and cross sections for particular excitation or population mechanisms. Since the γ-ray emission takes place *in flight*, the γ-ray detection arrays have to be sufficiently granular to allow for event-by-event Doppler reconstruction of the transition energies into the rest frame of the emitter.

Figure 6 shows the example of ^{36}Mg first studied with in-beam γ-ray spectroscopy following the two-proton removal from ^{38}Si projectiles [42]. The projectile-like reaction residues exiting the target were unambiguously identified and characterized by the S800 spectrograph. On the left, the upper spectrum shows the spectrum as detected in the laboratory frame with NSCL's highly segmented SeGA array (32 segments per detector) that covered a range of angles centred on 90° and 37°. The lower panel shows the spectrum event-by-event Doppler reconstructed into the rest frame of the projectile at v/c = 0.396. Two quantities enter into the Doppler reconstruction, the velocity of the emitter (^{36}Mg) and the γ-ray emission angle. The velocity of the projectile beam and the reaction residues, respectively, is known sufficiently accurate before and after the target from the magnetic rigidities of the beam transport systems and magnetic spectrometer setting, while the emis-

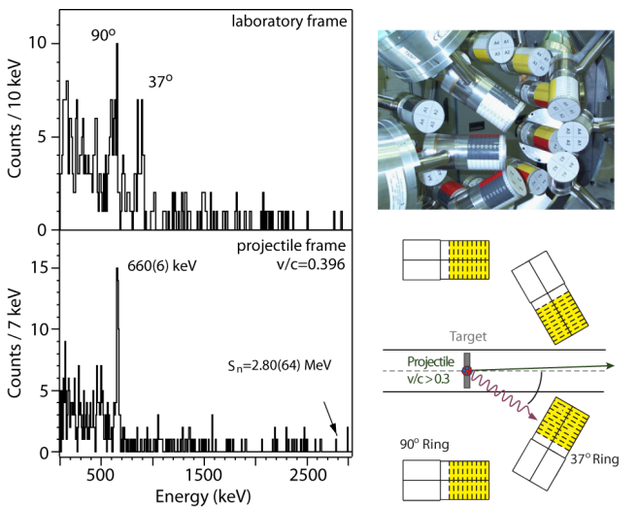

Figure 6. *Left: (top) Gamma-ray spectrum of ^{36}Mg populated in the two-proton knockout from ^{38}Si as detected in the laboratory frame and (bottom) event-by-event Doppler reconstructed into the rest frame of the emitter. The 660 keV transition is detected Doppler-shifted due to the emission in flight (v/c=0.396). The two peak structures in the top spectrum correspond to the detection of the γ rays in the SeGA detectors that covered a range of angles around 90° and 37°. Right: The corresponding γ-ray detection setup is shown as photograph (top) and schematically (bottom). The measurement was possible with a projectile beam of only 1,500 ^{38}Si per second and a cross-section of just above 0.1 mb for the production of ^{36}Mg [42].*

sion angle can be determined from the location of the detector segment that registered the highest γ-ray energy deposition. Figure 6 (right) shows a photograph of the SeGA array in the geometry used for the spectroscopy of ^{36}Mg and a more schematic view that illustrates the target position relative to the two rings of SeGA detectors. In-beam γ-ray spectroscopy programs with in-flight produced fast beams are presently pursued at NSCL/MSU in the United States, at GSI in Germany, at RIBF/RIKEN in Japan and at GANIL in France.

Perspective

Nuclear structure studies are a worldwide effort with contributions coming from complementary experimental investigations performed at different facilities. Excitation energies of rare isotopes often provide the first detailed information beyond the proof of existence of a rare nuclear species and its β-decay half life. Simple patterns emerge for the 2^+_1 states in even-even nuclei, revealing a powerful tool to sensitively track the changes of nuclear structure in exotic nuclei already at this modest level of information. Odd-A and odd-odd nuclei provide a window into the detailed interplay of single-particle structure and nucleon-nucleon correlations, serving as stringent benchmarks for nuclear models in the quest for a predictive model of nuclei across the nuclear chart. Progress in this endeavor relies on the close collaboration between experiment and theory, with feedback provided both ways. In-beam γ-ray spectroscopy with fast beams provides robust and sensitive approaches to study collective and single-particle degrees of freedom in the most exotic nuclei accessible. The future of rare-isotope studies is bright, as new powerful heavy-ion drivers have come into operation in Japan and are under construction in Europe and in the United States and very advanced γ-ray detection systems are online in the United States (GRETINA) and Europe (AGATA).

Acknowledgments

Discussions with B. Alex Brown are acknowledged. This work was partially supported by the National Science Foundation under Grant No. PHY-1102511.

References

1. T. Otsuka, *Phys. Scr*. T152 (2013) 014007.
2. T. Otsuka and A. Schwenk, *Nucl. Phys. News* 22(4) (2012) 12.
3. J. Dobaczewski et al., *Prog. Part. Nucl. Phys* . 59 (2007) 432.
4. K. Riisager, *Rev. Modern Phys*. 66 (1994) 1105.
5. M. G. Mayer, *Phys. Rev*. 75 (1949) 1969.
6. O. Haxel et al., *Phys. Rev*. 75 (1949) 1766.
7. A. Gade and T. Glasmacher, *Prog. Part. Nucl. Phys*. 60 (2008) 161.
8. B. Rubio and W. Gelletly, *The Euroschool Lectures on Physics with Exotic Beams, Vol. III Lecture Notes in Physics* 764 (2009) 99.
9. M. Block et al., *Phys. Rev. Lett*. 100 (2008) 132501.
10. M. W. Reed et al., *Phys. Rev. Lett.* 105 (2010) 172501.
11. M. Hunyadi and M. N. Harakeh, *Nucl. Phys. News* 18(1) (2008) 10.
12. B. A. Brown, *Lecture Notes in Nuclear Structure Physics, NSCL and Department of Physics and Astronomy*, Michigan State University (2011).
13. A. Ratkiewicz, Ph.D. Dissertation, Michigan State University, East Lansing, Michigan (2011).
14. National Nuclear Data Center, NNDC, http://www.nndc.bnl.gov/
15. E. K. Warburton, J. A. Becker, B. A. Brown, *Phys. Rev*. C 41 (1990) 1147.
16. O. Sorlin and M.-G. Porquet, *Prog. Part. Nucl. Phys*. 61 (2008) 602.
17. T. Glasmacher et al., Phys. Lett. B 395 (1997) 163.
18. B. Bastin et al., *Phys. Rev. Lett*. 99 (2007) 022503.
19. Y. Utsuno et al., *Phys. Rev.* C 86 (2012) 051301(R).
20. F. Nowacki and A. Poves, Phys. Rev. C 79 (2009) 014310.
21. A. Gade et al., *Phys. Rev. Lett*. 102 (2009) 182502.
22. R. Winkler et al., *Phys. Rev. Lett*. 108 (2012) 182501.
23. J. A. Tostevin, B.A. Brown and E.C. Simpson, *Phys. Rev*. C 87 (2013) 027601.
24. L. Gaudefroy and S. Grévy, *Nucl. Phys. News* 20(2) (2010) 13.
25. A. Huck et al., *Phys. Rev.* C 31 (1985) 2226.
26. R. V. F. Janssens et al., *Phys. Lett.* B546 (2002) 55.
27. J. I. Prisciandaro et al., *Phys. Lett.* B510 (2001) 17.
28. M. Honma et al., *Phys. Rev.* C 65 (2002) 061301.
29. D. Steppenbeck et al., *Nature* 502 (2013) 207.
30. J. Meng et al., *Phys. Rev.* C 65 (2002) 041302(R).
31. C. J. Lister et al., *Phys. Rev. Lett*. 59 (1987) 1270.
32. O. Sorlin et al., *Phys. Rev. Lett*. 88 (2002) 092501.
33. O. Sorlin et al., *Eur. Phys. J.* A 16 (2003) 55.
34. A. Gade et al., *Phys. Rev.* C 81 (2010) 051304(R).
35. M. Bernas et al., *Phys. Lett.* B 113 (1982) 279.
36. S. Rahaman et al., *Eur. Phys. J.* A 34 (2007) 5.
37. K. Langanke et al., *Phys. Rev.* C 67 (2003) 044314.
38. A. Gade and J.A. Tostevin, *Nucl. Phys. News* 20(1) (2010) 11.
39. A. Gade et al., *Phys. Rev*. C 74 (2006) 034322.
40. J. Papuga et al., *Phys. Rev. Lett*. 110 (2013) 172503.
41. S. R. Stroberg et al., *Phys. Rev*. C 86 (2012) 024321.
42. A. Gade et al., *Phys. Rev. Lett*. 99 (2007) 072502.
43. N. Aoi et al., *Nucl. Phys.* A805 (2008) 400c.